IDEA

Innovations Deserving
Exploratory Analysis Programs

Rail Safety IDEA Program

Minimization of Weld Failures by Means of Gas and Shrinkage Porosity Reduction

Final Report for
Rail Safety IDEA Project 38

Prepared by:
Francisco C. Robles Hernandez
S. Ray Taylor
Miad Yarali
Fernando D. Cortes Vega
University of Houston

February 2022

TRB TRANSPORTATION RESEARCH BOARD
The National Academies of
SCIENCES · ENGINEERING · MEDICINE

Innovations Deserving Exploratory Analysis (IDEA) Programs Managed by the Transportation Research Board

This IDEA project was funded by the Rail Safety IDEA Program.

The TRB currently manages the following three IDEA programs:

- The NCHRP IDEA Program, which focuses on advances in the design, construction, and maintenance of highway systems, is funded by American Association of State Highway and Transportation Officials (AASHTO) as part of the National Cooperative Highway Research Program (NCHRP).
- The Rail Safety IDEA Program currently focuses on innovative approaches for improving railroad safety or performance. The program is currently funded by the Federal Railroad Administration (FRA). The program was previously jointly funded by the Federal Motor Carrier Safety Administration (FMCSA) and the FRA.
- The Transit IDEA Program, which supports development and testing of innovative concepts and methods for advancing transit practice, is funded by the Federal Transit Administration (FTA) as part of the Transit Cooperative Research Program (TCRP).

Management of the three IDEA programs is coordinated to promote the development and testing of innovative concepts, methods, and technologies.

For information on the IDEA programs, check the IDEA website (www.trb.org/idea). For questions, contact the IDEA programs office by telephone at (202) 334-3310.

IDEA Programs
Transportation Research Board
500 Fifth Street, NW
Washington, DC 20001

Final Report

Minimization of Weld Failures by Means of Gas and Shrinkage Porosity Reduction

Submitted to

Rail Safety IDEA Program
Transportation Research Board
National Academies of Sciences, Engineering, and Medicine

Submitted by

Francisco C. Robles Hernandez
S. Ray Taylor
Miad Yarali,
Fernando D. Cortes Vega
Department of Engineering Technology
University of Houston
Houston, TX 77204-4021

February 23, 2022

Executive Summary

The objective of this work is to provide a new methodology to improve thermite welds. Thermite weld improvement is important because it is a major concern for the North American railways and it is crucial to meet the network demands in terms of safety, reliability and ridership operations. More specifically, the main objective of this work is to improve fatigue performance (i.e., strength when subjected to cyclic stress) by minimizing the two most common types of porosity, gas and shrinkage. Gas porosity is the result of the precipitation of oxygen during solidification, and shrinkage pores are due to thermal contraction combined with lack of melt feeding into the solidifying casting, which in this case is the thermite weld. To accomplish this objective, we have proposed a vibration technology that is applied during the solidification of the thermite welds to reduce the gas pores and refine the microstructure. The result is an improved weld material with superior mechanical properties. The work is divided into three major stages: *i*) design of experiments and thermal weld casting, *ii*) mechanical testing, optical microscopy, and *iii*) analysis and reporting of results. Due to the expense associated with performing first-time experiments on numerous thermite welds, we used a statistical method, Design of Experiments (DOE), to efficiently explore the process variables of our vibration system. The purpose of DOE is to determine the specific variable that control a multi-variable process. In addition, we developed a rail weld simulation device to use in our laboratory so that we could pre-test the vibration device and explore the controlling variables. This information allows for a more efficient exploration of the vibration process when applied to thermite welds. The operational variables that we consider for the design of experiments are vibration frequency, vibration force, vibration orientation and the distance of the vibrator from the weld. The first set of experiments was conducted in our laboratory scale simulator to understand the fluid mechanics of the vibration on a liquid. The experiments were performed using water containing marker. Water has very similar fluid properties (e.g. kinematic viscosity) to liquid steel. In addition, the added marker provided a method to track the specific motion of the water (or molten steel) when vibration is applied. The simulation results permitted the identification of the most important operating parameters to be tested in 16 experimental welds. Three additional welds were cast following current standard practices and used as controls. The results indicate that the treatment is effective and improves the service life of the welds. Results from thermite welds treated with our vibration process show improvements in strength of up to 12% and a reduction in porosity. The porosity reduction has an expected improvement on the fatigue endurance limit of up to 30%. The treated welds were inspected using the protocols and recommended practices in American Railway Engineering and Maintenance-of-Way Association (AREMA). These tests demonstrated that the vibration treatment is suitable for revenue service use as it does not have negative effects on welds. The vibration parameter that has the greatest benefit is frequency, followed by the vibrating force. The other two parameters, orientation and distance between the vibrator and the weld, have lesser influence. This report summarizes the methodology followed in order to propose a successful weld treatment.

Contents

List of Figures

List of Tables

Appendix: Lists of Figures and Tables

Introduction

This investigation seeks to identify new methods for rail life extension by improving the fatigue resistance of thermite welds. Rail weld failure can result from a wide variety of reasons, such as porosity, defects (e.g., slag, flints), columnar grains, hot tears, lack of fusion, improper finishing (e.g., poor grinding), inclusions, and entrapped sand, among others [1]. The objective of this project is to investigate a method to improve track performance by developing higher performing thermite welds.

Fatigue cracks can nucleate at different sites. The nucleation sites that are the focus of this study are voids in the form of pores, developed mainly by gas, shrinkage, or their combinations. The proposed approach for void minimization is mechanical vibration induced through vibrator motors during the solidification process. The liquid metal vibration process described here was first applied to a weld simulation device developed in our laboratories. The information learned from these lab simulations was then applied to 16 treated thermite welds. The treated welds were then compared to three (3) untreated control welds (i.e., reference samples). In order to have a statistically significant reference, we labeled the reference sample representing the average of the three control sample tests as Sample 17 in this report. The weld treatments were selected based on the design of experiments (DOE) to determine the controlling variables. Here we present the results of the entire project, including a statistical analysis to show the significance of the results and to demonstrate the effects and benefits of vibration on thermite welds.

Stage I: Design of Experiments and Thermal Weld Casting

In this report, we complement the results presented in all previous reports for this project. We also include the Task I (kickoff meeting) participation.

Task I: Kickoff meeting with expert review panel: A project kick-off meeting will be held with the expert review panel and Rail Safety IDEA Program Manager.

The kickoff meeting was held on January 19, 2020 and was chaired by Dr. V. Fitzpatrick and attended by Dr. F. Robles. The list of attendees included:

University of Houston
S. R. Taylor (Co-PI)
M Yarali, PhD Candidate

Industrial Partner
Lois Flenner, Product Manager
ATW – North America

Project Advisor
Brad Kerchof, Director
Norfolk Southern Railway

Expert Advisory Panel
C. I. Garcia, Professor
University of Pittsburgh

R. Ordoñez Olivares, Senior Engineer
Ellwood Quality Steels

Daniel A. Bjork
DABCO CONSULTIN, LLC
Consultant

The PI (Dr. Robles) introduced the topic and explained the overall idea of the project. Each advisor and committee member introduced themselves and explained their experience and participation. Dr. V. Fitzpatrick described the timetable, deliverables and commitments from the committee.

It is important to mention that Railtech Boutet has changed its name to Pandrol. Additionally, Mr. Louis Flenner is no longer with Pandrol and potentially no longer a participant in this committee.

Task 2. The following are the variables used for the DOE for the simulation test that was later conducted on thermite welds at the Pandrol facilities in Napoleon, Ohio:

1. Location on Rail 1 (close, far),
2. Location on Rail 2 (close, far)
3. Frequency (high, low),
4. Impact loading conditions (minimum, maximum),
5. Motor position (parallel, perpendicular),

Note: the meaning of "*close*" is a distance of 6 inches from the weld, while "*far*" is 6 feet from the weld. In some experiments (e.g., full factorial) both vibrators were placed simultaneously close or far from the weld, while in other cases one was close and the other was far.

Table A 1 in the Appendix shows the full factorial DOE for the case of five variables. DOE is a statistically based method that allows one to develop an experimental matrix to identify the controlling variables in a multi-variable process. A full factorial model, which can determine all combinations of variable interactions, requires 2^n experiments (2^5 in this case) where "*n*" is the number of variables. Therefore, we carried out 32 experiments using a weld simulation device developed in our lab to examine the actual effect of each parameter on thermite weld solidification. The full factorial test was completed using the simulation device shown in Figure 1A . Due to the accuracy of a fractional factorial DOE and prior agreements with Pandrol on thermite weld quantity, we performed a 2^{n-1} (2^4) fractional factorial design, or 16 thermite weld test samples (Table A 1, Run 1-16). In addition to these 16 test samples, 3 untreated control samples were provided by Pandrol for reference. The average results of the reference samples are identified in this report as Sample 17. The set up for the lab simulations, the respective images for the physical model, and the LabView analyzed images are presented in Figure 1. The rail used in this experiment is 136 RE, which is manufactured by Steel Dynamics. This rail was selected due to its common use on Class I railroads, which is the main target of the technology presented herein.

Task 3. Build and Assess Vibration System

Figure 1b presents the technical drawings for the vibration motors used in this work. The same motors were used in both the lab and field experiments. The motors used in this work can generate frequencies

of up to 40 Hz with amplitudes of up to 400 lbf of load. The device shown in Figure 1 is a weld simulation device that can be used safely in the laboratory. It allowed us to explore weld variables in a safe and inexpensive manner. The fastening system consisted of Pandrol clips and Pandrol plates bolted down to a 4-inch-thick plywood platform with the intention to create conditions like those over wood ties. The motors are attached to the rails using a custom fastening system. In Figure 1c, one can see the liquid cell used for the vibration analysis. This clear acrylic cell allowed the observation of vibration interaction within the weld space. We optimized the distance between rails for the UH-simulation test to 3 inches. The three-inch gap between the rails in our physical simulation device optimized the laboratory conditions for digital imaging. This optimization is based on a combination of parameters associated with (1) the minimum requirements for data acquisition and (2) the amount of data required for the image processing to obtain meaningful results over the simulations. We do understand that rail weld gaps are usually 1-1.5 inches not 3 inches. Figure 1d presents an image of the laboratory cell during a vibration treatment. This image was acquired using a laser with a wavelength of 532 nm, polyamide seeding particles which are highlighted by the laser, to simplify identification with the high speed camera. The polyamide seeding particles are used as markers within the water to reveal the motion of the water. Figure 1e shows the simulated wave interaction within the water as the vibration conditions change. Water is key for the experiments because it possesses a similar kinematic viscosity as liquid steel [2-5] and it is transparent. Therefore, water represents a similar condition to molten steel used in thermite welds. Numerical simulations can also be conducted online using the following platform: https://www.desmos.com/calculator/zz5mgkexjj. The mathematical model used to determine the wave interactions is presented in the following:

The vibration in each rail can be represented with a sine wave:

$$f(x) = A\sin(Bx + E) \qquad \text{Eq. 1}$$

$$g(x) = C\sin(Dx + F) \qquad \text{Eq. 2}$$

where A and C are the amplitude, B and D are the frequency, and E and F are the phase shift.

Figure 1f-g show the digitalized images of the physical model as documented with the camera and analyzed on the PIV-lab software. The image processing allowed for the generation of the data presented in the last three columns of Table A 1 in the Appendix. These parameters, or ranges, will be compared with the mechanical test results to optimize the conditions at a later stage. These parameters are the indicators for both the severity of the process and how the process contributes to the mechanical improvements of the welds.

Task 4. Produce Treated Thermite Welds

We visited the Pandrol facility in Napoleon, Ohio to pour all of the welds indicated in the fractional factorial DOE (experiments 1-16 in Table A 1 in the Appendix). Figures 5 and 6 show examples of the welds cast in the Pandrol facility. A more descriptive collage of images is presented in Figures A1-A10 in

the Appendix. The fractional factorial weld experiments carried out at Pandrol are the most important samples for understanding the effect of the test parameters on the mechanical properties of the welds. Both the fractional (tests 1-16 highlighted in green) and full factorial (tests 1-32) tests are described in the Appendix in Table A 1. A full factorial design examines all combinations of all proposed variables, while a fractional factorial design examines a smaller number of combinations of all proposed variables. Fractional factorial design is effective because it is unlikely that a process is controlled by the simultaneous interaction of all variables, which in this case is five (5). A fraction factorial DOE is designed to reduce the effort without sacrificing statistical soundness or accuracy. The last three columns in Table A 1 (velocity, vorticity, and shear (see Figure 2)) are the results from the physical simulations at UH. The black sphere in Figure 2 represents a polyamide particle in liquid water; similar effects are expected when two waves interact in the liquid or when a wave and a solidifying particle in the molten thermite weld. The data was analyzed using box plots to represent each of the simulations as a function of the three variables with the most fundamental effects on the liquid cell: velocity, vorticity, and shear. Velocity is the determined based on the motion of the polyamide particles in water in a specific direction, shear is a measure of friction within the fluid or between the fluid and polyamide particles, and vorticity is a measure of the development of a circular path within the fluid. For a more detailed description, see Figure 2. Graphs were plotted for each test and are shown in Figure 3. In these graphs, it can be seen that frequency is the process variable that provides the highest velocity and shear force as well as the second lowest vorticity. This combination of outcomes is desirable for the optimized treatment condition because it accomplishes the lowest void content and highest fatigue resistance. If the vorticity is low, the amount of potential entrapped gases decreases.

Entrapped gases are a well-known topic in castings [1, 2]. The effects of vibration usually have benefit to castings by reducing or eliminating the presence of pores. One can associate the vibration test with that of shaking a can of carbonated beverage and releasing the dissolved CO_2. From our laboratory weld simulation results, both shear and vorticity can be used to predict the effects of vibration on casting soundness or porosity reduction. Both results seem to agree, and they are complementary for the purpose of improving the soundness of welds. However, an increase in the vorticity may result in higher density of entrapped air, which must be avoided. These results are also evaluated using metallography of the welds and then compared based on an analysis of variance (ANOVA or t-test). The results from Figure 1f-g are used to reproduce a box plot that includes all of the velocity vectors present in such figures. Note that each data 'point' in the matrix shown in Figure 4a is a vector where the length represents the magnitude, or the intensity for the velocity, vorticity, or shear. The direction of the vector represents the direction of the quantity.

In Figure 3, the magnitude of the velocity is plotted for all 32 lab simulation tests using velocity components along the x-direction (u) and y-direction (v) extracted from Figure 1f-g. According to this figure, high velocity can be achieved in tests where frequency and impact loading conditions are high, while decreasing these two parameters causes velocity to drop. This can be observed in Figure 3 and Figure 4 where all tests from most severe to least severe are compared to determine the effect of each parameter on velocity, vorticity, and shear. In this figure, only one parameter changes while others are constant, therefore we can conclude from this figure that frequency has the highest impact on the

velocity as Figure 3e shows. Vorticity (ω) and shear stress (τ) are also calculated based on u and v to study the effect of the DOE parameters on them. As Figure 3b, d illustrates, vorticity and shear stress are close to zero when frequency and impact loading conditions are minimum, and they increase as these two parameters increase.

Figure 4 shows a comparison among severe vibration conditions and a summary of how these conditions change as a function of frequency, force, orientation, and location of the vibrators with respect to the weld. In Figure 4a, b we can see the difference among a test conducted under mild conditions to one conducted under severe conditions. These maps are the weld simulator results made in our laboratory to prove the effect of the various conditions tested and are further summarized in Figure 4c. In Figure 4a and b, it is possible to observe the significant differences between mild and severe vibration conditions. These differences are later utilized for the determination of the most important parameters in the vibration process. From these images, the importance of the laboratory simulations is clearly seen as they represent a starting point in terms of field-testing parameters. From here, we can propose optimized test treatments for the molten thermite. In summary, we have determined that frequency is the most important parameter for melt treatment, followed by wave amplitude or force, orientation (mounting) and distance (position). The orientation indicates how the wave travels within the rail and is then transmitted to the liquid.

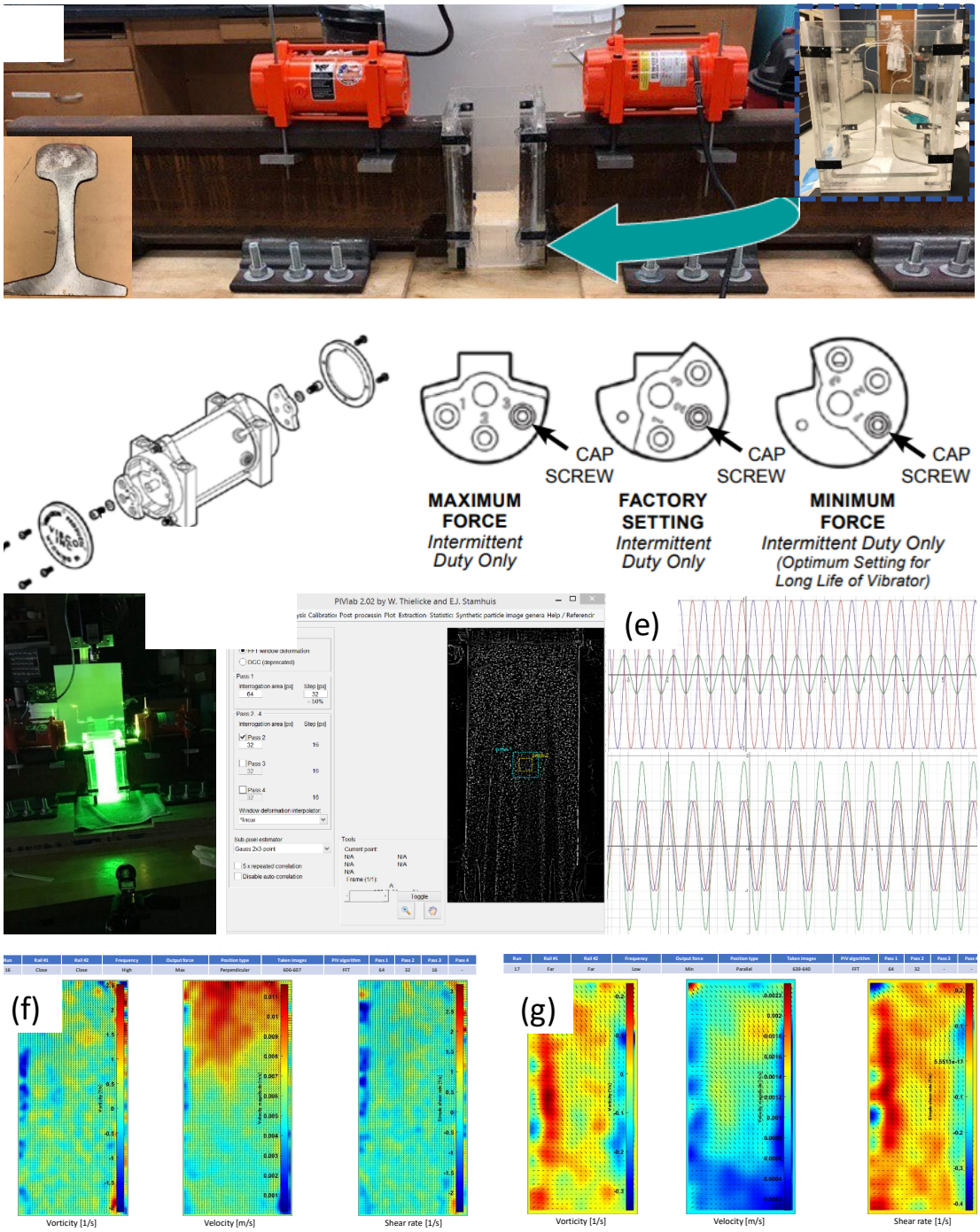

Figure 1. (a) rail-vibrators assembly, (b) blueprints for the vibrator motors, (c) laser–cameras set up for the assembly shown in (a), (d) data acquisition system on PIBlab software, (e) vibration interactions for moderate and severe conditions (f-g) simulated moderate and severe vibration environments respectively.

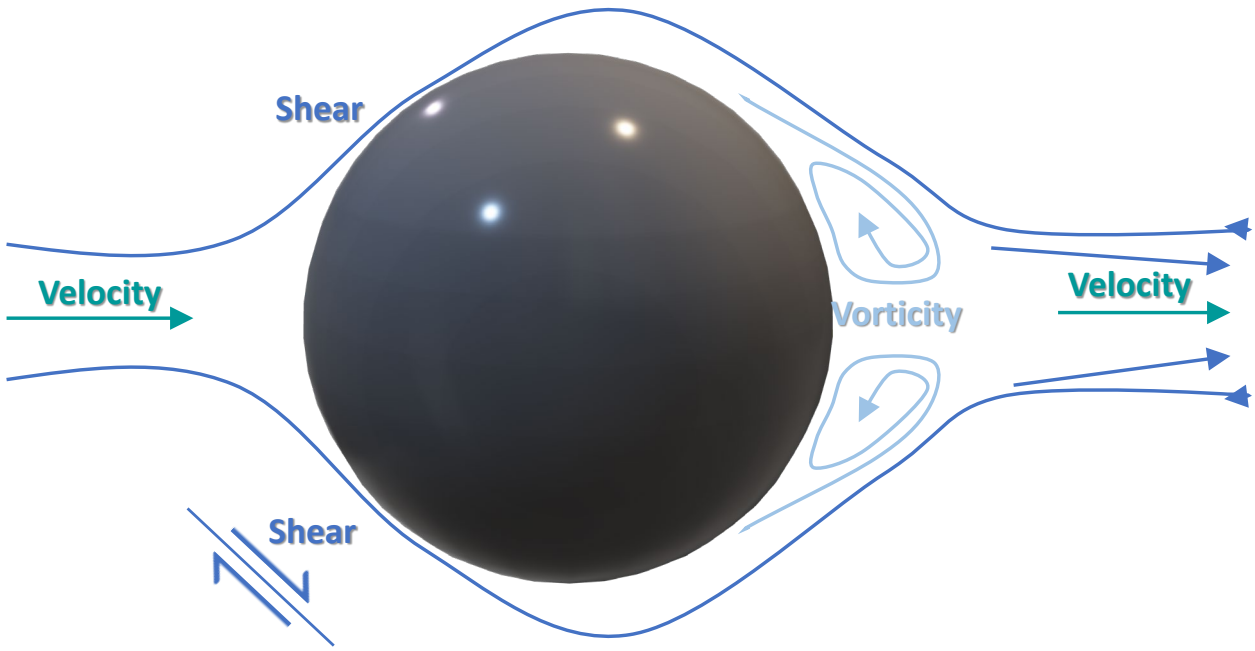

Figure 2. Sketch showing the differences among velocity, vorticity, and shear.

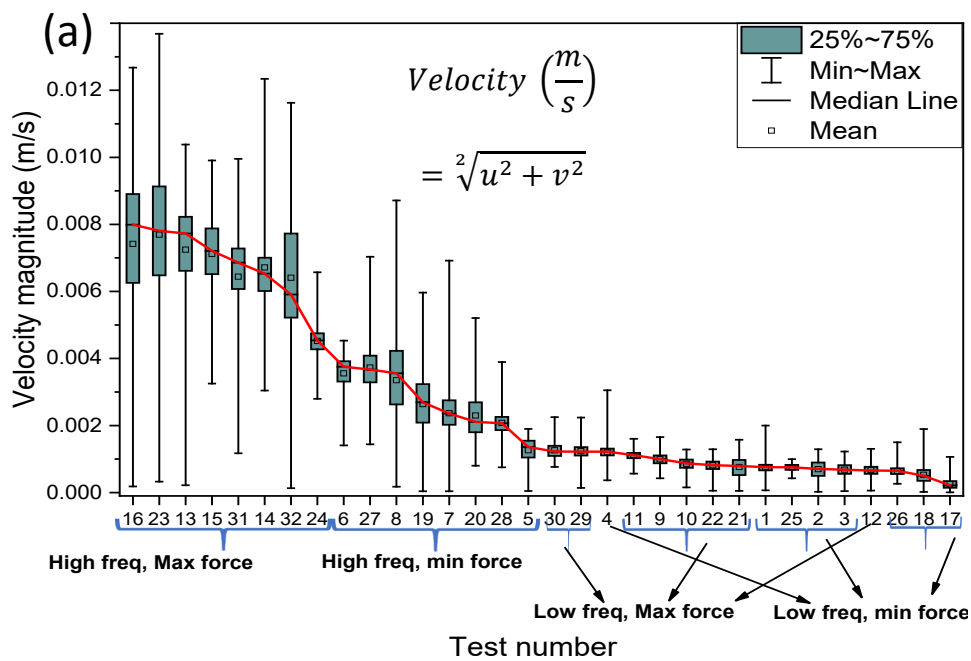

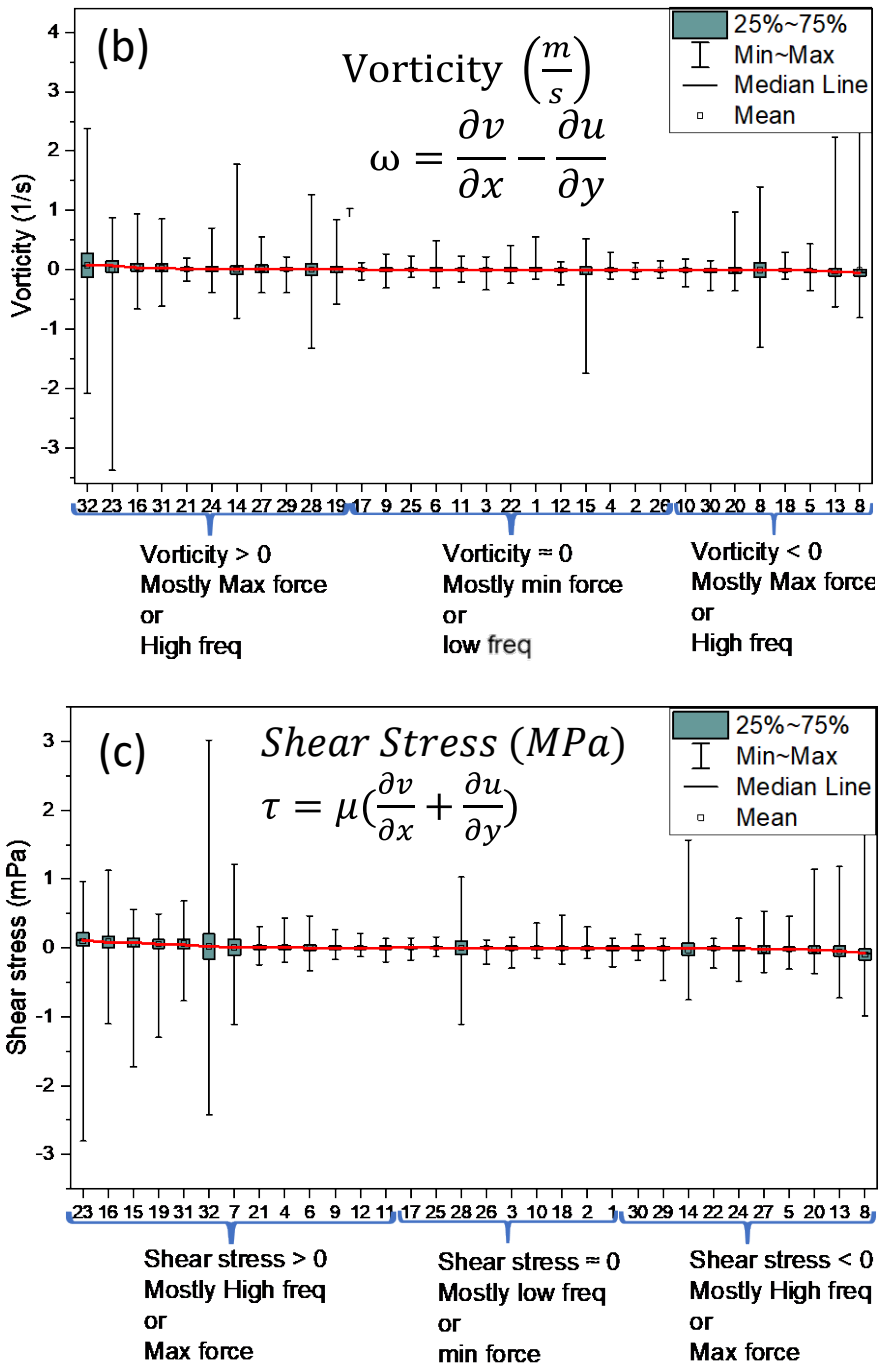

Figure 3. Simulation test results for the full design of experiments using a full functional factorial for five variables (32 tests). Summary of the simulated test severity as a function of (a) velocity, (b) vorticity, and (c) shear.

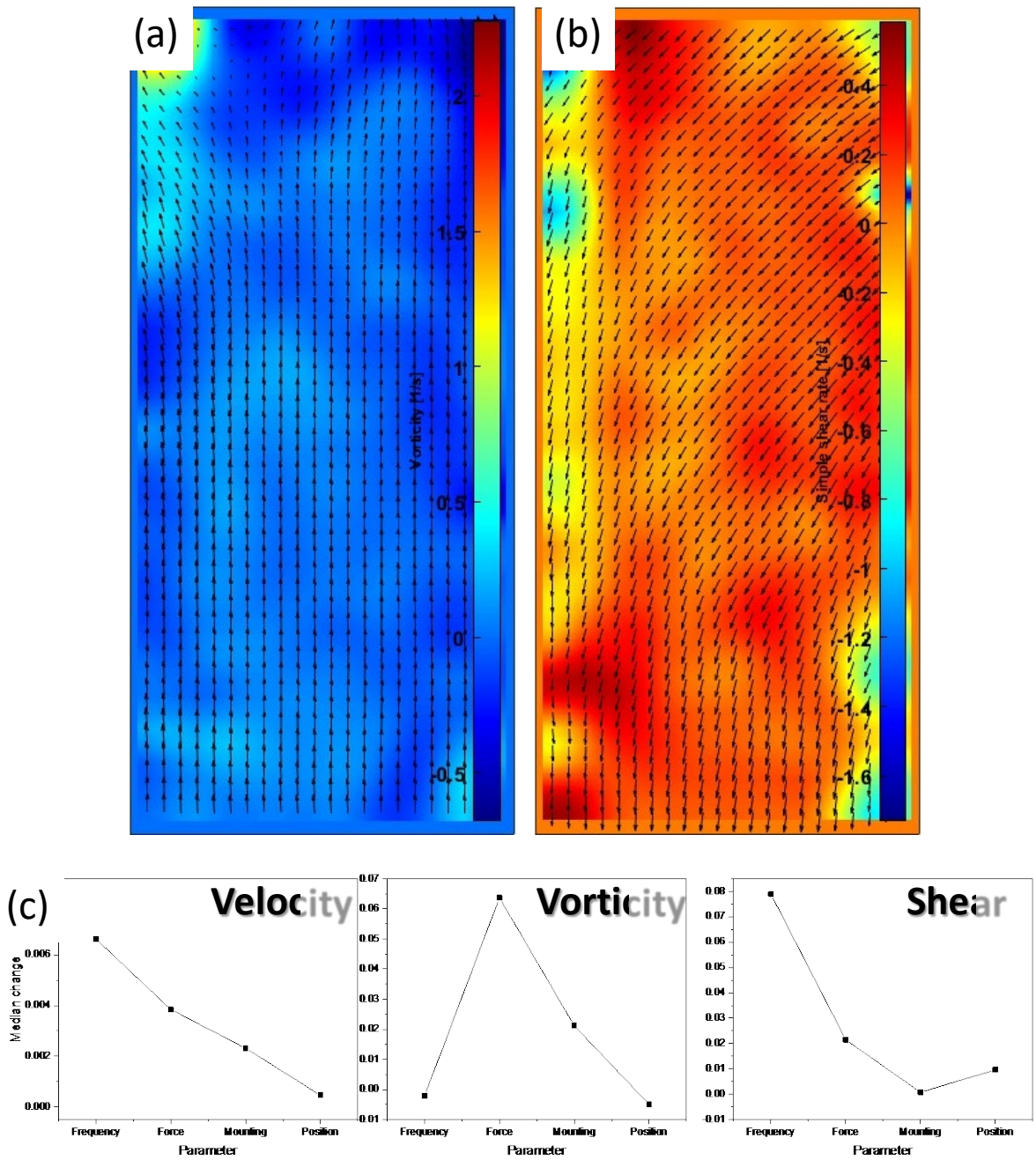

Figure 4. Examples of simulated tests conducted under (a) mild and (b) severe conditions and (c) a summary of the importance of the test conditions for the various experiments. Note: (a) and (b) are graphs showing the velocity profile in the liquid melt in the presence of the vibration severity. The graph's color indicates severity: the blue is mild and the yellow-orange-red is increased severity. The vector's length represents its amplitude, and the direction indicates the flow or stirring of the molten weld.

Table 1. Summary of the nondestructive (ultrasonic and visual inspection) testing.

Run	Rail #1	Rail #2	Frequency	Force	Position type	Flashing	Magnetic particle examination		Ultrasonic examination		Result
							Void/porosity/shrinkage	comments	Void/porosity/shrinkage	comments	
1	Far	Far	Low	Min	perpendicular	Around the collar on both sides	Some voids in the tear drop area, possible shrinkage	-	Some voids in the tear drop area, possible shrinkage	-	good
2	Close	Far	Low	Min	parallel	Around the collar on both sides And on the base	-	Alignment is off on the base, crack under ball of rail, baseplate possibly off-center	-	Alignment is off on the base, crack under ball of rail, baseplate possibly off-center	Good/crack
3	Close	Close	Low	Min	parallel	Around the collar on one side And on the base	Shrinkage in head at side riser	Alignment is off on the base	Shrinkage in head at side riser	Alignment is off on the base	good
4	Close	Close	Low	Min	perpendicular	Around the collar on one side prevalently, some flashing on opposite side	Shrinkage in head at tear drop on both sides, small voids	-	Shrinkage in head at tear drop on both sides, small voids	-	good
5	Far	Far	High	Min	parallel	Around the collar on one side prevalently, some flashing on opposite side	Shrinkage in head at tear drop on both sides, small voids	-	Shrinkage in head at tear drop on both sides, small voids	-	good
6	Close	Far	High	Min	perpendicular	Around the collar on both sides	Small voids in the tear drop area, possible shrinkage	-	Shrinkage in head at tear drop on both sides, small voids	-	good
7	Close	Close	High	Min	perpendicular	Around the collar on one side, minimal on opposite side, flashing in the base	Minimal shrinkage in head at tear drop on both sides, small voids	-	Minimal shrinkage in head at tear drop on both sides, small voids	-	good
8	Close	Close	High	Min	parallel	Around the collar on one side prevalently , no flashing on opposite side	Porosity in head at tear drop on both sides, small voids larger on one side	Bulky mass on the base, fused risers	Porosity in head at tear drop on both sides, small voids larger on one side	Bulky mass on the base, fused risers	good
9	Far	Far	Low	Max	parallel	Around the collar on one side prevalently, some flashing on opposite side at the base	porosity/voids in head at tear drop on both sides, voids larger on one side	-	porosity/voids in head at tear drop on both sides, voids larger on one side	-	good
10	Close	Far	Low	Max	perpendicular	Minimal flashing around the collar on both sides	-	-	-	-	good
11	Far	Far	Low	Max	perpendicular	Around the lower fillet and base on one side prevalently, some flashing on opposite side	No porosity/voids in head at tear drop on both sides	-	No porosity/voids in head at tear drop on both sides	-	good
12	Close	Close	Low	Max	parallel	Around the collar on both sides	No porosity/voids in head at tear drop on both sides	Weld was ground to specification	No porosity/voids in head at tear drop on both sides	Weld was ground to specification	good
13	Far	Far	High	Max	perpendicular	Around the collar on both sides, thick flashing on the base of one side	-	Risers fused in the web area, large steel formation	-	Risers fused in the web area, large steel formation	good
14	Close	Far	High	Max	parallel	Around the collar on both sides, prevalent around base-fillet and ball-fillet areas	Some porosity around the small riser/tear drop	-	Some porosity around the small riser/tear drop	-	good
15	Close	Close	High	Max	parallel	Around the collar on both sides, prevalent around base-fillet area, thick flashing along the base on one side	Some porosity around the small riser/tear drop	-	Some porosity around the small riser/tear drop	-	good
16	Close	Close	High	Max	perpendicular	Around the collar on both sides, prevalent around base-fillet area	Some porosity around the small riser/tear drop	-	Some porosity around the small riser/tear drop	-	good
17	Non-treated weld (standard)					Slight flashing around collar on one side, prevalent around web area	Some porosity around the small riser/tear drop	-	Some porosity around the small riser/tear drop	-	

Task 5. Ultrasound Testing

An image of a thermite weld being cast at Pandrol in Napoleon, Ohio is presented in Figure 6. The collage in Figure A1-A10 in the Appendix provides the details from the rail cutting, vibration testing, melt pouring/casting, and final grinding. An important characteristic of the process is presented in Figure 7, where one can see a deep sink along the feeding system. This unusual sink is an empiric indicator of the benefits of the vibration operation as a result of improved liquid metal feedability to the welds. In other words, we could empirically say that the deeper the sink, the better the treatment. Therefore, it is expected that the vibrated welds will have improved mechanical properties. Examples of welds treated under the scope of this work and commercial welds are given in Figure 7. The collage of images from Figure 5 to Figure 7 demonstrate that the motors fit the rails and that the set up can either be placed in front of or behind the *"A"* frame. Note that the *"A"* frame is only a reference and not a requirement for a successful vibration treatment. The motors can be located as close as 4 to 6 inches to the weld. We recommend that the motors be no more than 10 ft. from the weld, however, this can vary depending on many parameters and track conditions. The summary of the ultrasonic testing and visual inspection evaluations is presented in Table 1.

The non-destructive testing (NDT) analysis demonstrates that the vibration method used does not have a detrimental effect on the thermite weld process or casting. Therefore, we can conclude that the vibration process generally has no negative effects on the welds. Although flashing is not desirable, it is encountered routinely and was also observed in our control samples. However, flashing has a simple solution. Pandrol and other companies have special techniques and molds to prevent flashing; therefore, flashing is not considered a detrimental effect because it is possible to eliminate it. The flashing is presented in Figure 8. The results indicate that the weld treatment, vibration method, is considered suitable for field applications.

Figure 5. Image of an "A" frame along the railway track. The image was taken from Pandrol's website[†]

A collage of images in the Appendix shows the reference welds as well as the set up for weld vibration at different stages. Figures A1 and A2 present the images of a control weld (no vibration, not provided to UH). Figure A3 and A4 are welds treated by vibration. The rail base shows comparable flashing among the control and the vibration test samples. On the other hand, the web and head show flashing. This flashing is the result of a compromised joint between the mold and the rail as presented in Figure 8.

[†] https://www.pandrol.com/us/products/

Figure 6. Thermite welding test site and track panel used for the actual weld test. The image shows the complete set up during rail/mold preheating.

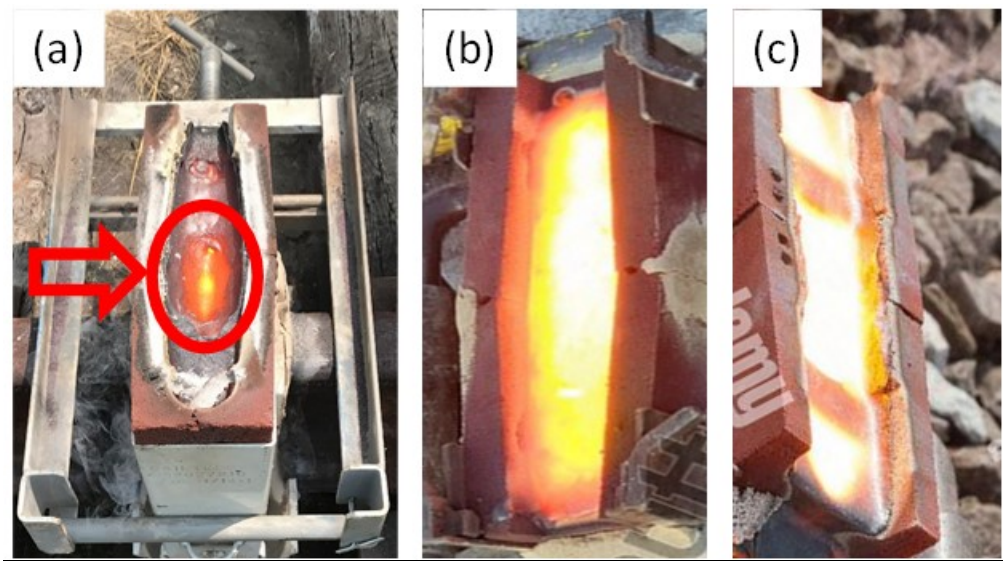

Figure 7. Thermite weld's top view showing the solidifying surface of the red-hot state of the molten alloy. The examples include: (a) this work (vibrated weld), (b) Shutter Stock[‡], and (c) Alamy[§]. Note: it is not the intention of this work to indicate what weld is better or to show or give any impression about the products, but rather to demonstrate that vibration has a direct effect on feedability and is observed in the "sink" over the weld's surface. The images were selected from online sources. Note: the sink is highlighted in (a) with a red oval and an arrow.

[‡] https://www.shutterstock.com/image-photo/railroad-thermit-welding-works-1200273211
[§] https://c8.alamy.com/comp/2C79BCB/thermit-welding-on-rail-track-in-the-uk-2C79BCB.jpg

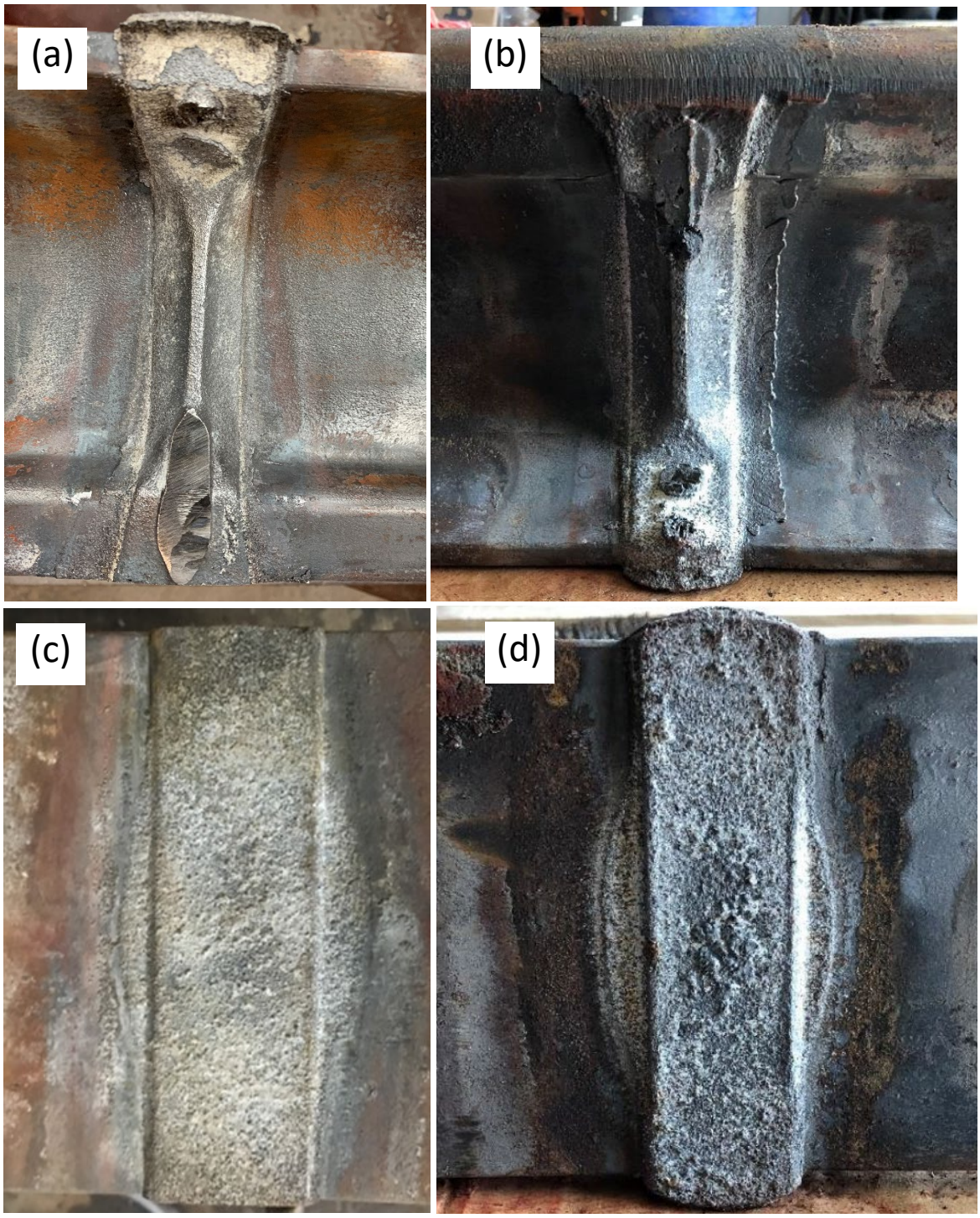

Figure 8. Images/examples of a reference sample (a) without testing in the absence of flashing and (b) a sample with flashes on the web and head. The flashes at the base of the rail are comparable among that in the (c) reference and (d) vibration treated sample.

Stage II. Mechanical Testing and Optical Microscopy

Task 6. Sample Extraction for Mechanical Testing

The samples for mechanical testing were extracted from treated welds by Pandrol. The data from these test samples will determine the best welding conditions. All of the reported mechanical properties are or belong to the welded section. The extracted samples were subjected to tests that included optical microscopy, scanning, Charpy impact, and tensile tests. Hardness tests were conducted along the weld region over the tensile test samples using the Rockwell C hardness scale following ASTM E18. All tests followed standard procedures as recommended by the ASTM. For more information we include other views of the same technical drawings in the Appendix (Figure A11, A12). The tensile, Charpy, and metallographic samples were extracted from all the welds and are presented in Figure 9. Figure 10 shows the locations and standards that will be used to analyze each type of sample.

Figure 9. (a) An example set of samples extracted for mechanical testing.

Porosity Analysis

Treated and control (non-treated) samples were optically examined to determine the porosity/void content. Samples were polished as follows:

1. Grind with 240, 320, 400 and 600 grit SiC paper
2. Rinse with ethanol, dry with compressed air
3. Fine polishing with 5 μm alumina powder (28 g/1 oz)
4. Sonicate in ethanol for 5 mins, rinse with ethanol
5. Fine polishing with 1 μm alumina powder
6. Sonicate in ethanol for 5 mins, rinse with ethanol
7. Fine polishing with 0.05 μm alumina powder
8. Sonicate in ethanol for 5 mins, rinse with ethanol, dry with compressed air and keep in desiccated chamber

A metallographic sample approximately 1 cm x 1 cm x 1cm was taken from each weld. The exact location is indicated by number 4 in Figure 10. The sample characteristics and location are identified as item 4. One plane of this section was polished for metallurgical observation. The samples were analyzed under the optical microscope using 10 images per sample at 100X magnification. The 10 images were sufficient to demonstrate statistical significance. The images were then analyzed using ImageJ software to calculate porosity counts and sizes. The results from all 10 images were added together to have a representative and statistically reproducible representation of the weld microstructure. This number of fields and magnification was selected because it is reproducible and reaches a confidence level that meets reproducibility. The software was calibrated by the scale bar on the images. All pores were identified based on grey shade contrast to distinguish between pores and inclusions as presented in Figure 12.

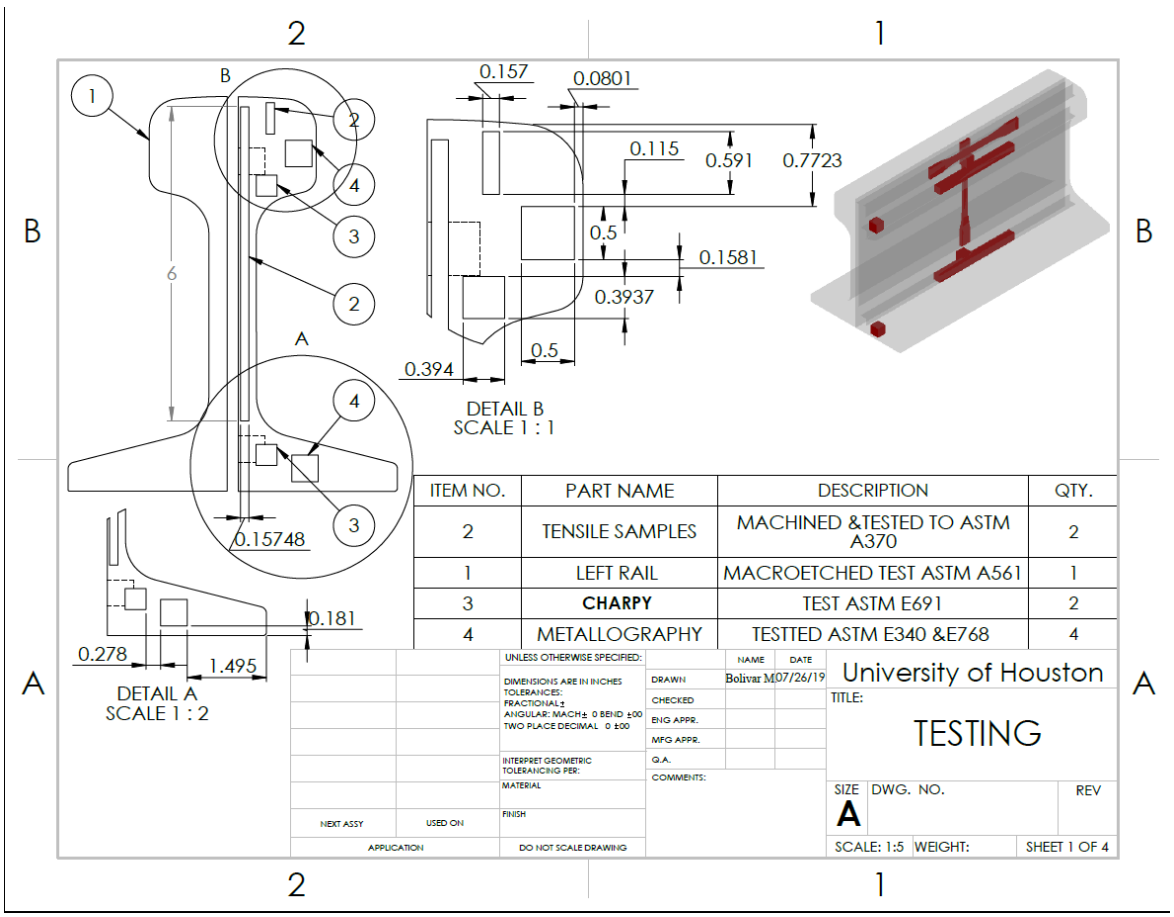

Figure 10. Protocol for the preparation of metallographic and mechanical testing samples.

The features of interest in this work, pores and inclusions, were discernible by grey tone differences using ImageJ software. It is important to note that gas pores are mainly round while shrinkage pores are more elongated, so it is also possible to differentiate them with the naked eye on the microstructures. However, it is less tedious and more straightforward to use ImageJ software since some of the features are combinations of gas and shrinkage adding complexity to the analysis. The differences between these

pores are shown in Figure 12. No limitation on pore size and circularity were applied. All pores were analyzed comprehensively with ImageJ software. As Figure 13 and Figure 14 show, Sample #2, which was prepared with low frequency and minimum impact loading conditions, has smaller pores and less porosity by 36% and 43% respectively compared to the control sample. In addition, pores and voids start to merge with increasing frequency and impact loading conditions as samples number 11, 15 and 16 illustrate. However, they still contain a lower number of voids than the untreated sample. The conditions for the samples shown in Figure 13 are given in Table 2. It is important to mention that the samples in Table 2 and Figure 13 are randomly selected to show a representative example.

The tensile test results are presented in Figure 11. This graph shows the benefits of mechanical vibration treatment of thermite welds on tensile properties. From Figure 11, one can see that there are two behaviors in terms of strength performance. In one case, the strength is improved, and in the other case, the strength is reduced. This concept is important because some of the vibration treatment conditions are beneficial for the improvements of strength, and others are not. In order to maximize the benefits of the thermite weld vibration treatment, it is necessary to optimize the treatment conditions. The results in Figure 11 make evident that the wave amplitude is the main parameter that affects strength. This is attributed to the increase in the shear forces or friction within the molten thermite that help break the solidifying particles (also called dendrites) promoting grain refinement. Grain refinement, or reduction, is reported as a benefit to the overall properties of the weld. It also improves feedability within the solidifying alloy and is known as a strengthening mechanism. Grain refinement has been used for decades as an indicator of mechanical property improvement, which was originally proposed by the Hall-Petch equation [6]. The porosity analysis is added to Figure 11 to demonstrate that yield strength is almost independent of porosity. However, porosity is a main contributor to fatigue life. Thus, strength and fatigue can be treated individually using thermite weld vibration treatments.

The hardness results were performed using the ASTM E18-20 standard for the Rockwell C test. There is up to a 20% increase in hardness as a result of the thermite weld vibration treatment. The hardness measurements reported are the result of three measurements made along the weld on the tensile test sample.

The Charpy test was carried out following the ASTM D6110-18 standard. The Charpy test was performed using only one sample. From the results, it is evident that most samples show clear improvement in terms of impact toughness. The sample with the highest toughness is Sample 3 showing an 86% benefit over the control, followed by Sample 5 with a 57 % benefit. These results are encouraging. In order to get more realistic values, it is recommended that future work determine the fracture toughness (KIc ASTM E399-20) instead of impact toughness.

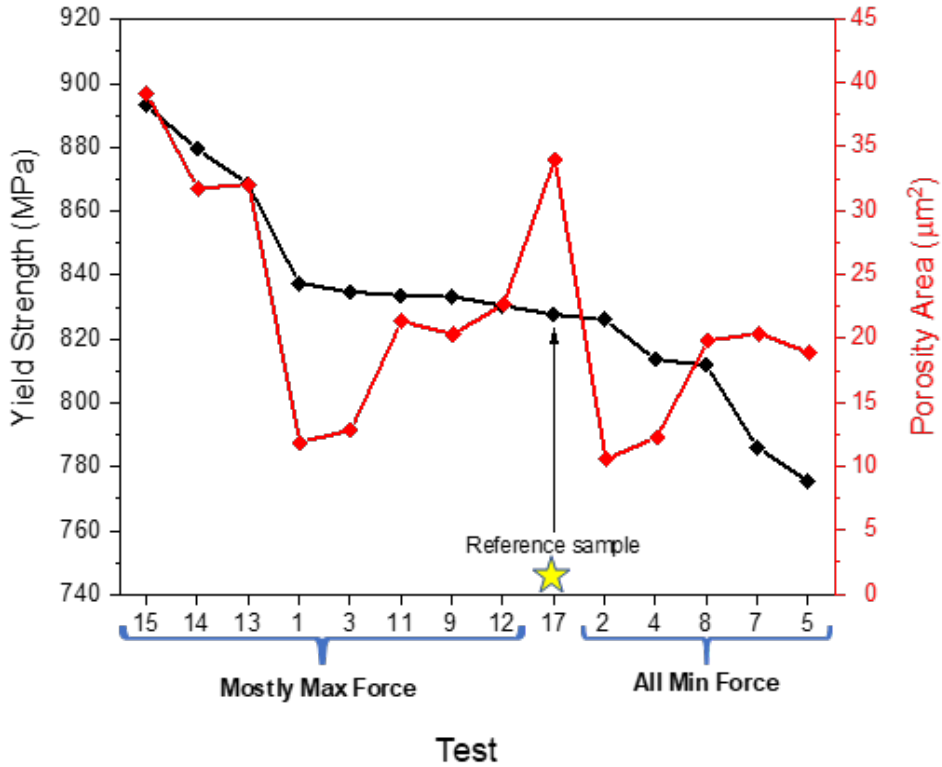

Figure 11. Summary of the tensile test results as performed on the reference and treated thermite welds.

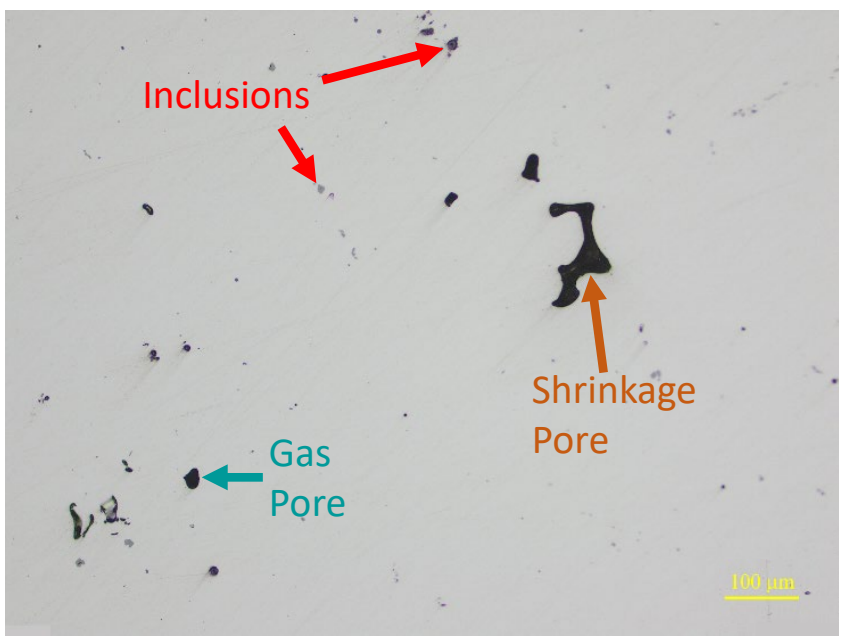

Figure 12. Optical metallographic image showing characteristic features in the microstructure. The importance herein is to demonstrate that it is relatively easy to differentiate among inclusions and pores, which is a programmable feature in ImageJ software. Image was taken from Sample 9.

Table 2. Summary of the conditions in which Samples 2, 11, 15 and 16 were prepared.

Run	Rail #1	Rail #2	Frequency	Force	Position type
2	Close	Far	Low	Min	parallel
11	Far	Far	Low	Max	perpendicular
15	Close	Close	High	Max	parallel
16	Close	Close	High	Max	perpendicular

Table 3. Hardness and Charpy Impact test results for the reference and thermite weld treated samples.

Test Sample	**Hardness** (HRc)	**Charpy Impact** ft-lb
1	37.8 ±1.7	7
2	34.8 ±1.3	8
3	35.5 ±0.6	13
4	33.3 ±1.3	9
5	35.5 ±1	11
7	35.5 ±0.6	9
8	35.8 ±1	8
9	37 ±0.8	8
11	35.5 ±0.6	8
12	36.3 ±1	8
14	38 ±1.8	9
15	38 ±2.2	9
17[♨]	31.8 ±1	7±1

[♨] Sample 17 is the average of the 3 reference samples.

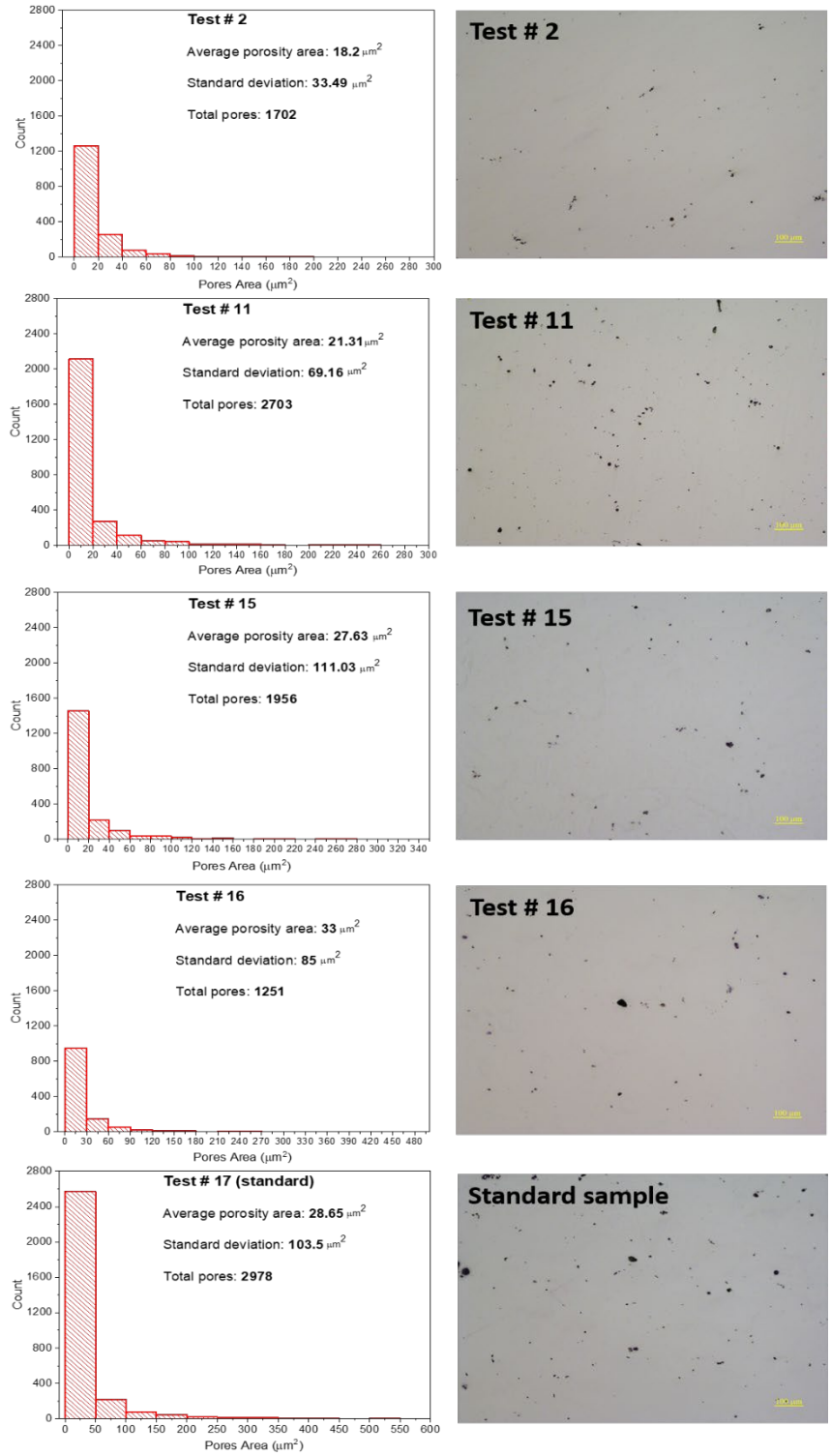

Figure 13. Porosity analysis for treated and Control samples. Note: Sample 17 presented herein represents the average of the three samples.

Stage III. Analysis of Results

The analysis of the results for porosity as a function of treatment severity is presented in Figure 14. In this figure we can see two parameters as the most important for fatigue and mechanical properties of the thermite welds. These two parameters are the number of pores and the pore size. While the number of pores is critical, the pore size has more dramatic effects. For example, the same pore area divided among smaller pores versus a single larger pore has completely different effects. Both act as stress concentrators, but the larger pore intensifies the stress concentration. This phenomenon is known as the stress intensity factor and is presented in Figure 14b. Stress concentration can be explained as the number of times the applied force (or stress, force per unit area) is multiplied by the presence of defects, in this case pores. This effect was proposed by Griffith [7] and Irwin [8], two main contributors to the field of fracture mechanics. In summary, the phenomena that we present in this analysis is the effect of defect size on the integrity of structural components. From Figure 14b, one can see an inverse effect of defect size and stress concentration. As the size of a defect increases, the concentration of the stresses increases in the same direction. Now, it is important to clarify that we are using the most simplified approach. There are other approaches that involve geometry, but this is beyond the scope of the present work. In the presence of a defect, the stress concentrates, promoting crack initiation and crack growth that may result in sudden or catastrophic failure. As a general rule, catastrophic failure is a condition that should be prevented or avoided, particularly in welds.

The Griffith model proposes that a component under uniaxial tension, i.e., pulled from both ends in opposing directions, has a drop in its mechanical properties in the presence of cracks. In this case we can determine the effects of strength in the presence of cracks using the model shown in Eq. 3.

$$\sigma_f = \sqrt{\frac{2E\gamma}{\pi c}} \qquad \text{Eq. 3}$$

Where: σ_f is the critical strength at failure,

E is the young's modulus,

γ is the surface energy,

"*c*" is the crack length. For internal cracks it is "2*c*", for surface cracks is "*c*".

This model (Eq. 3) predicts the effects on brittle materials under limited plastic deformation. In the case of welds, the crack initiation is conducted under fatigue or cyclic loading. A more adequate model to predict fatigue is the Paris equation. The Paris equation is used to predict the number of cycles that a component sustains before it fails catastrophically. Once the fatigue crack ("shinny" surface in Figure 15) reaches a size long enough (also called "critical" size), the failure occurs as a sudden process with limited

to no plastic deformation. At that point, the stress conditions have reached the σ_f value, i.e., the critical strength, and the component fails under plain strain conditions that are typically observed on welds. The plain strain is typical of brittle failure, such as glass, where the failure leaves a flat surface followed by a sharp edge at approximately 90˚. Here, we are not implying that welds behave as glass, but rather that under some circumstances, materials behave in a brittle manner and have the tendency to fail under similar conditions. This concept can be directly translated into a typical brittle failure with the characteristics of "river marks" and "chevron patterns" which point towards the site of crack initiation (in Figure 15); these characteristics are comparable to the "fissure" in our analysis of pores. The chevrons and the river marks are typically used to identify the site of crack initiation that is located opposite to their growth.

On the positive side of the vibration treatment, the fatigue performance of our samples was modeled using the Murakami equation [9], presented in Eq. 4.

$$\sigma_w = \frac{1.43(75+HV)}{\left(\sqrt{Area}\right)^{1/6}} \qquad \text{Eq. 4 [9]}$$

Where σ_w is the fatigue performance or endurance limit,

HV is the hardness in Vicker's scale,

Area, in microns or µm, is the particle size for defects smaller than 1.4 mm or 1,400 µm in length

As per Eq. 4, one can say that the endurance limit decreases as the pore defect size increases. One concept in the Murakami model that makes it relevant to our work is that by using the square root of the pore area (*e.g.*, length or diameter), the geometry of the pore either becomes irrelevant or the geometry is meaningless and only the length matters. This gives the particle a shape factor that is conventionally established as length over width. In the case of the Murakami concept, all defects have a shape factor of 1. This concept is relevant mainly to square or circular defects and, in our case, the gas pores are usually circular, illustrating this concept perfectly. The shrinkage pores, on the other hand, generally have irregular geometries due to being combined between contraction effects and entrapped gases as shown in Figure 12.

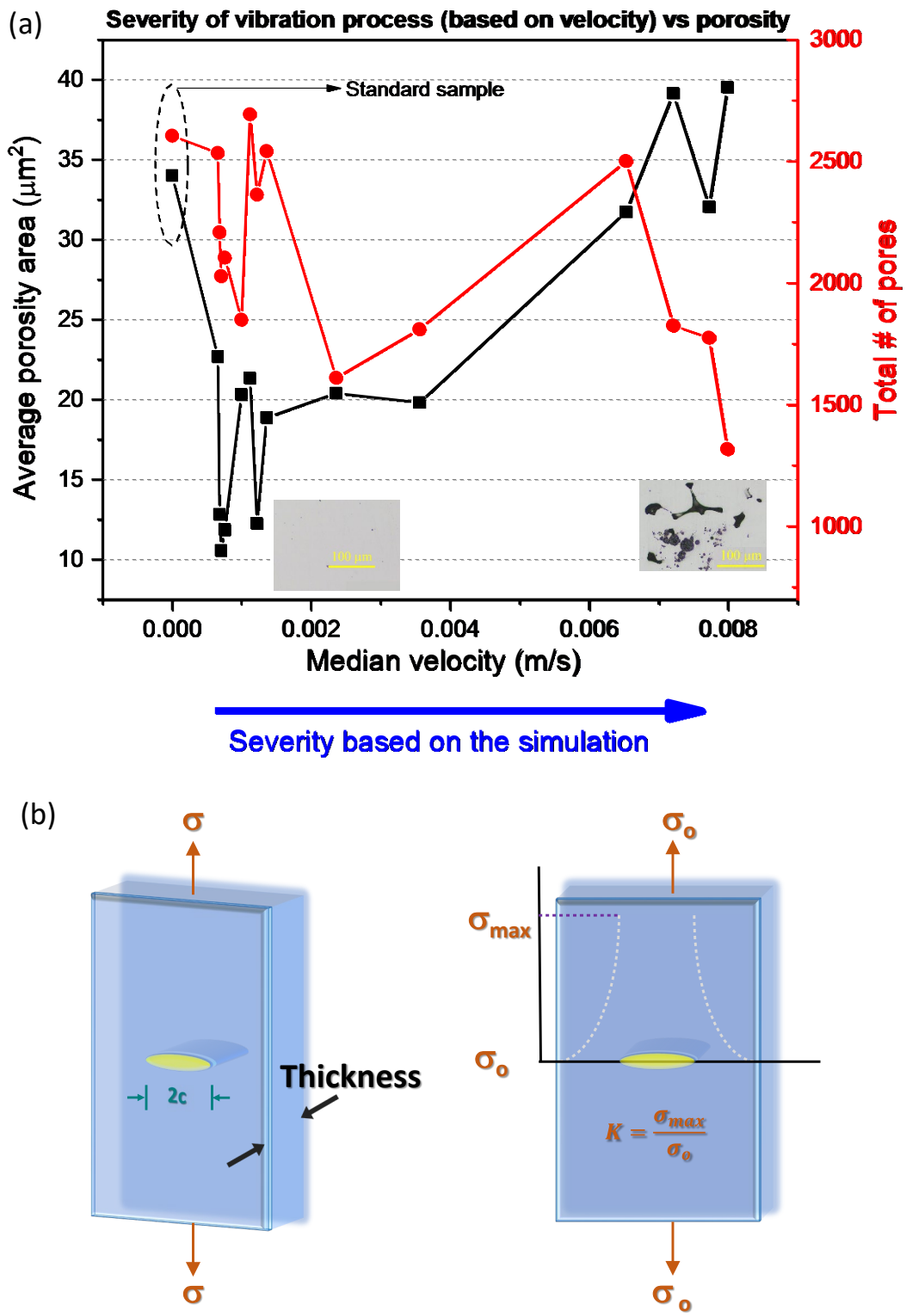

Figure 14. (a) Severity of vibration process vs porosity and (b) Griffith sketch demonstrating the effects of cracks in structural components.

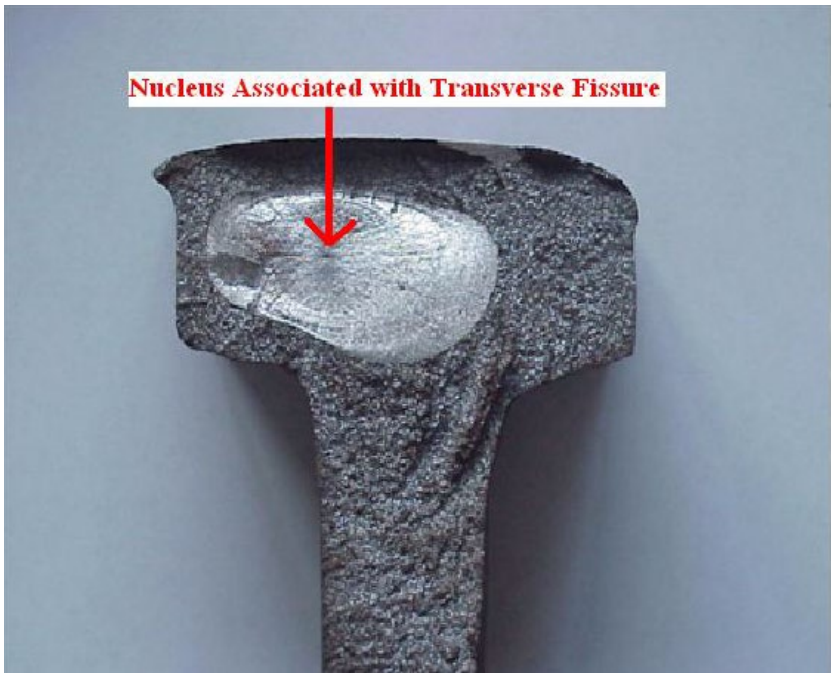

Figure 15. Detailed fracture at a defect. The original "polished" surface is characteristic of crack growth under fatigue conditions and initiated at a defect, in this case identified as a fissure. Image taken from the FRA Track Inspector Rail Defect Reference Manual.[**]

Figure 16 shows the effects of porosity on the fatigue performance of the investigated samples. In this figure, it is evident that all the vibration treatments benefit the fatigue performance. In all cases, we have a potential overall reduction of the pore sizes on the treated samples. Based on the results presented in Figure 16, it is evident that we can predict an average improvement of 30% in the fatigue limit or endurance limit. This is a significant improvement that can considerably increase the track integrity and lifetime of welds. This number relates mainly to crack initiation, which is the most important parameter in terms of fatigue performance. Therefore, based on the initial results from this research, the vibration method is highly recommended for the improvement of the fatigue life of thermite welds.

[**] https://railroads.dot.gov/sites/fra.dot.gov/files/fra_net/19052/Final%20FRA%20Rail%20Manual%20July%2029%202015_031716.pdf

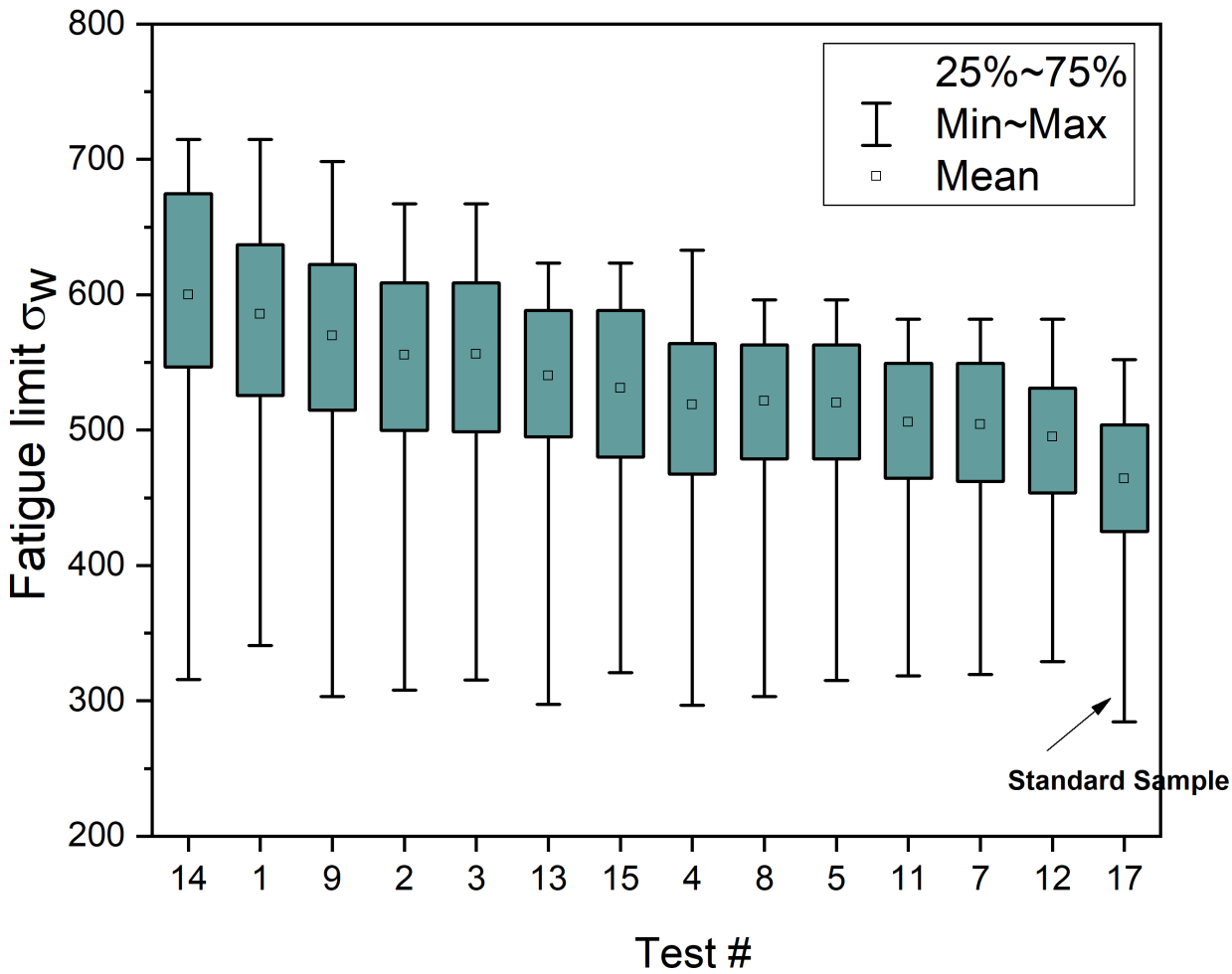

Figure 16. Fatigue results and performance improvement for the tested samples.

In summary, based on the DOE, the results validate the correctness of our physical simulator (Figure 1) and further demonstrate that mechanical tests follow the predictions from the lab experiments. Frequency is the most important parameters to treat the welds are frequency and force. The effects of all vibration parameters are summarized in Table 2. It is important to note that the results found in the simulator system at the University of Houston and the results from the mechanical testing agree. This validates our laboratory weld simulator, which now provides an easily accessible, low-cost method to explore best treatment conditions and parameters for the weld treatment. A new and unexpected finding is that strength and fatigue are independent. Fatigue benefits more from high frequency treatment due to porosity reduction, while strength improves from higher force or wave amplitude through a microstructure refinement mechanism. Parameters with lesser effect are the location and orientation of the vibration sources. In general, the results are an excellent starting point to extend this effort to more in-depth tests and potential commercialization.

Table 4. Summary of the statistical analysis for the vibration treatment severity and mechanical improvements of welds.

T-Test	Most significant variable
Velocity	Frequency
Vorticity	Force
Shear stress	None
Porosity area	Force
Absorbed energy	None

Summary

A vibratory method to improve the mechanical integrity of thermite welds was assessed. Prior to the manufacture of thermite welds, the controlling variables of this method were assessed through the development of a weld simulator and the analytical method, design of experiments (DOE). Using the weld simulator and DOE, a full factorial design using five (5) process variables totaling 32 (2^5) experiments were performed under laboratory conditions. The results from these simulations allowed us to rule out one process variable, *i.e.*, distance. We found that moving the vibrators closer or further from the weld either simultaneously or separately had no effect on vibration severity. Therefore, the resulting experimental matrix of 2^4 (16) samples was used to produce thermite welds by Pandrol with our vibratory process. Additionally, three control samples were also provided by Pandrol. Based on an analysis of porosity, Charpy impact strength, tensile strength and predicted fatigue properties, we can conclude that the frequency and the amplitude of the vibration have the strongest effects on the melt treatment and have the highest potential to achieve optimum conditions. The most important process parameters are the frequency of the vibration source and vibration amplitude (force). Wave orientation, which is related to the motor orientation with respect to the rail, has a moderate effect. The other control parameters are not as relevant, particularly the distance of the source from the weld. This result suggests that our vibration system can be placed either near the weld (6-10 inches) or as far behind as 6 to 10 ft from the weld, allowing a comparable outcome. This by itself is a significant finding, as it gives the welder's crew the freedom to locate the vibrator within 5 ft or more from the weld without compromising the vibration effect. Additionally, the vibration direction when oriented perpendicular to the rail provides a relative enhancing effect. While wave orientation is not as important as frequency or amplitude, it should not be ignored. Although the NDT results demonstrate success in the test, we still must eliminate flashing. This can be solved in two different ways: (*i*) the use of alternative molds that are designed to minimize this problem or (*ii*) reducing the wave amplitude. In our case, the second approach is a better choice because lower amplitudes permit to use the current commercial molds already approved by AREMA. As confirmed in the porosity analysis, essentially all the processing conditions tested using the vibratory method produce welds with reduced porosity. The next step in this

work is to tune this process, perform fatigue and slow bending tests, and conduct full-scale demonstrations at a railroad site or FAST-TTCI[††].

References

1. Hernandez, F.C.R., J.M.H. Ramírez, and R. Mackay, *Al-Si Alloys: Automotive, Aeronautical, and Aerospace Applications*. Al-Si Alloys: Automotive, Aeronautical, and Aerospace Applications. 2017. 1-237.
2. Gupta, D., S. Chakraborty, and A.K. Lahiri, *Asymmetry and oscillation of the fluid flow pattern in a continuous casting mould: A water model study.* ISIJ International, 1997. **37**(7): p. 654-658.
3. Lawson, N.J. and M.R. Davidson, *Oscillatory flow in a physical model of a thin slab casting mould with a bifurcated submerged entry nozzle.* Journal of Fluids Engineering, Transactions of the ASME, 2002. **124**(2): p. 535-543.
4. Brighton, A., et al. *Methodology of water modeling and submerged-entry nozzle (SEN) design for bloom casting with mold electromagnetic stirring (MEMS)*. in *AISTech - Iron and Steel Technology Conference Proceedings*. 2014.
5. Garcia-Hernandez, S., et al., *Numerical optimization of nozzle ports to improve the fluidynamics by controlling backflow in a continuous casting slab mold.* ISIJ International, 2013. **53**(10): p. 1794-1802.
6. Li, Y., A.J. Bushby, and D.J. Dunstan, *The Hall–Petch effect as a manifestation of the general size effect.* Proceedings of the Royal Society A: Mathematical, Physical and Engineering Sciences, 2016. **472**(2190): p. 20150890.
7. Griffith, A.A., *The Phenomena of Rupture and Flow in Solids.* Philosophical Transactions of the Royal Society of London. Series A, Containing Papers of a Mathematical or Physical Character, 1921. **221**: p. 163-198.
8. Irwin, G.R., *Closure to "Discussions of 'Analysis of Stresses and Strains Near the End of a Crack Traversing a Plate'" (1958, ASME J. Appl. Mech., 25, pp. 299–300).* Journal of Applied Mechanics, 2021. **25**(2): p. 300-301.
9. Tajiri, A., et al., *Fatigue Limit Prediction of Large Scale Cast Aluminum Alloy A356.* Procedia Materials Science, 2014. **3**: p. 924-929.

[††] https://www.ttci.tech/test-tracks/htl

Appendix

*Table A 1. Full factorial design of the experiments***

	Variables				Responses				
					Simulation				
Run	Rail 1	Rail 2	Frequency	Force	Position type	Velocity	Vorticity	Shear Stress	Porosity Area	Absorbed Energy
1	Far	Far	Low	Min	Perpendicular	$7.6*10^{-4}$	$-1.2*10^{-3}$	$-31*10^{-3}$	11.88	7
2	Close	Far	Low	Min	Parallel	$7.1*10^{-4}$	$-7.6*10^{-3}$	$-7.3*10^{-3}$	10.57	8
3	Close	Close	Low	Min	Parallel	$6.8*10^{-4}$	$-6.5*10^{-4}$	$-1.3*10^{-3}$	12.83	13
4	Close	Close	Low	Min	Perpendicular	$1.2*10^{-3}$	$-6.1*10^{-3}$	$6.6*10^{-3}$	12.26	9
5	Far	Far	High	Min	Parallel	$1.4*10^{-3}$	$-1.3*10^{-2}$	$-1.9*10^{-2}$	18.88	11
6	Close	Far	High	Min	Perpendicular	$3.8*10^{-3}$	$-4.1*10^{-4}$	$1.6*10^{-3}$	-	-
7	Close	Close	High	Min	Perpendicular	$2.4*10^{-4}$	$-1.1*10^{-2}$	$9.3*10^{-3}$	20.4	9
8	Close	Close	High	Min	Parallel	$3.6*10^{-3}$	$-5.1*10^{-2}$	$-7.6*10^{-2}$	19.82	8
9	Far	Far	Low	Max	Parallel	$1*10^{-2}$	$1.9*10^{-3}$	$1.1*10^{-3}$	20.33	8
10	Close	Far	Low	Max	Perpendicular	$8.7*10^{-4}$	$-9.3*10^{-3}$	$-1.4*10^{-3}$	-	-
11	Far	Far	Low	Max	Perpendicular	$1.1*10^{-4}$	$-4.8*10^{-4}$	$2*10^{-3}$	21.35	8
12	Close	Close	Low	Max	Parallel	$6.6*10^{-4}$	$-2.3*10^{-3}$	$2.6*10^{-3}$	22.68	8
13	Far	Far	High	Max	Perpendicular	$7.7*10^{-3}$	$-3.2*10^{-2}$	$-4.4*10^{-3}$	32.05	-
14	Close	Far	High	Max	Parallel	$6.5*10^{-3}$	$1.2*10^{-2}$	$-1.9*10^{-3}$	31.74	9
15	Close	Close	High	Max	Parallel	$7.2*10^{-3}$	$-4.4*10^{-3}$	$8.2*10^{-2}$	39.16	9
16	Close	Close	High	Max	Perpendicular	$8.0*10^{-3}$	$3.4*10^{-2}$	$8.2*10^{-2}$	39.54	-
17	Far	Far	Low	Min	Parallel	$2.1*10^{-4}$	$4.4*10^{-3}$	$5*10^{-3}$		
18	Far	Close	Low	Min	Parallel	$5.0*10^{-4}$	$-1.2*10^{-2}$	$-4.3*10^{-3}$		
19	Close	Far	High	Min	Parallel	$2.7*10^{-3}$	$5*10^{-3}$	$5.5*10^{-2}$		
20	Far	Close	High	Min	Parallel	$2.1*10^{-3}$	$-1.0*10^{-3}$	$-2.8*10^{-2}$		
21	Close	Far	Low	Max	Parallel	$7.9*10^{-4}$	$1.3*10^{-2}$	$8.2*10^{-3}$		
22	Far	Close	Low	Max	Parallel	$8.1*10^{-4}$	$-6.6*10^{-3}$	$-5.6*10^{-3}$		
23	Far	Far	High	Max	Parallel	$7.8*10^{-3}$	$6.8*10^{-2}$	1.2		
24	Far	Close	High	Max	Parallel	$4.5*10^{-3}$	$1.2*10^{-2}$	$-3.6*10^{-3}$		
25	Close	Far	Low	Min	Perpendicular	$7.5*10^{-4}$	$8.6*10^{-5}$	$2.7*10^{-3}$		
26	Far	Close	Low	Min	Perpendicular	$6.5*10^{-4}$	$-8.3*10^{-4}$	$-5.8*10^{-4}$		
27	Far	Far	High	Min	Perpendicular	$3.7*10^{-3}$	$8.7*10^{-4}$	$-1.8*10^{-2}$		
28	Far	Close	High	Min	Perpendicular	$2.1*10^{-3}$	$6.5*10^{-3}$	$8.3*10^{-4}$		
29	Far	Close	Low	Max	Perpendicular	$1.2*10^{-3}$	$7.3*10^{-3}$	$-3.7*10^{-3}$		
30	Close	Close	Low	Max	Perpendicular	$1.2*10^{-3}$	$-9.4*10^{-4}$	$-2.4*10^{-3}$		
31	Close	Far	High	Max	Perpendicular	$6.9*10^{-3}$	$2.8*10^{-2}$	$4.6*10^{-2}$		
32	Far	Close	High	Max	Perpendicular	$5.9*10^{-3}$	$7*10^{-2}$	$2.2*10^{-2}$		

** Vorticity is a vector that provides a local measure of the instantaneous rotation of a fluid parcel. Velocity is a vector that describes the direction and speed of a fluid parcel. Shear rate is the amount of change of velocity at which one layer of fluid passes over an adjacent layer.

Figure A 1. Collage of the thermite welding test site and track panel used for the welds

Figure A 2. Collage of the thermite welding test site rail cut to generate the gap for the weld.

Figure A 3. Collage of the thermite welding test site mold placement.

Figure A 4. Assembly to assess the boundary conditions.

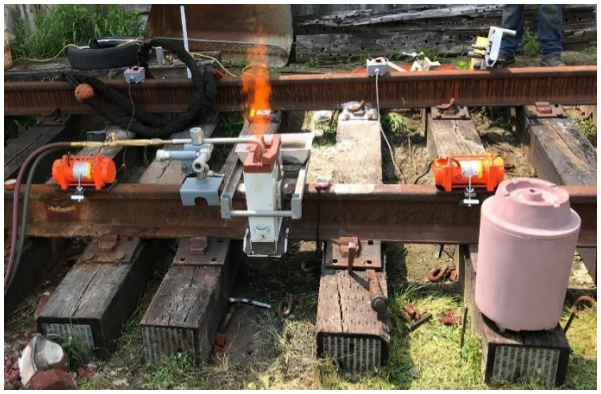

Figure A 5. Mold preheating.

Figure A 6. Weld sectioning.

Figure A 7. Weld pouring/casting and slag removal.

Figure A 8. Hot weld with sink.

Figure A 9. Hot weld with sand core removed.

Figure A 10. Grinded weld with risers.

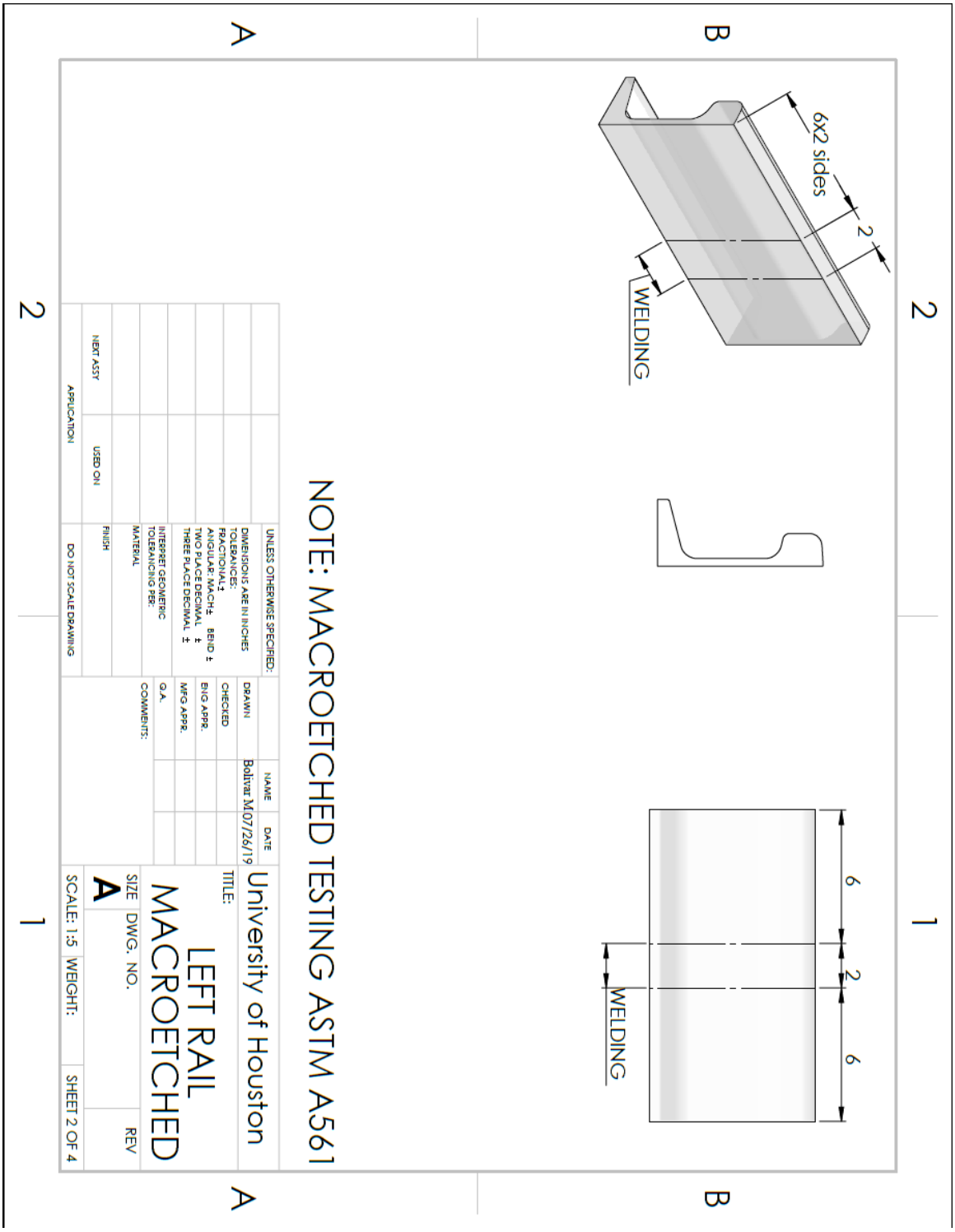

Figure A 11. Sketch of the weld and its main dimensions. Note: the actual gaps were made of 1.25 inches. Here we use 2 inches to elucidate the potential for wide gap welds.

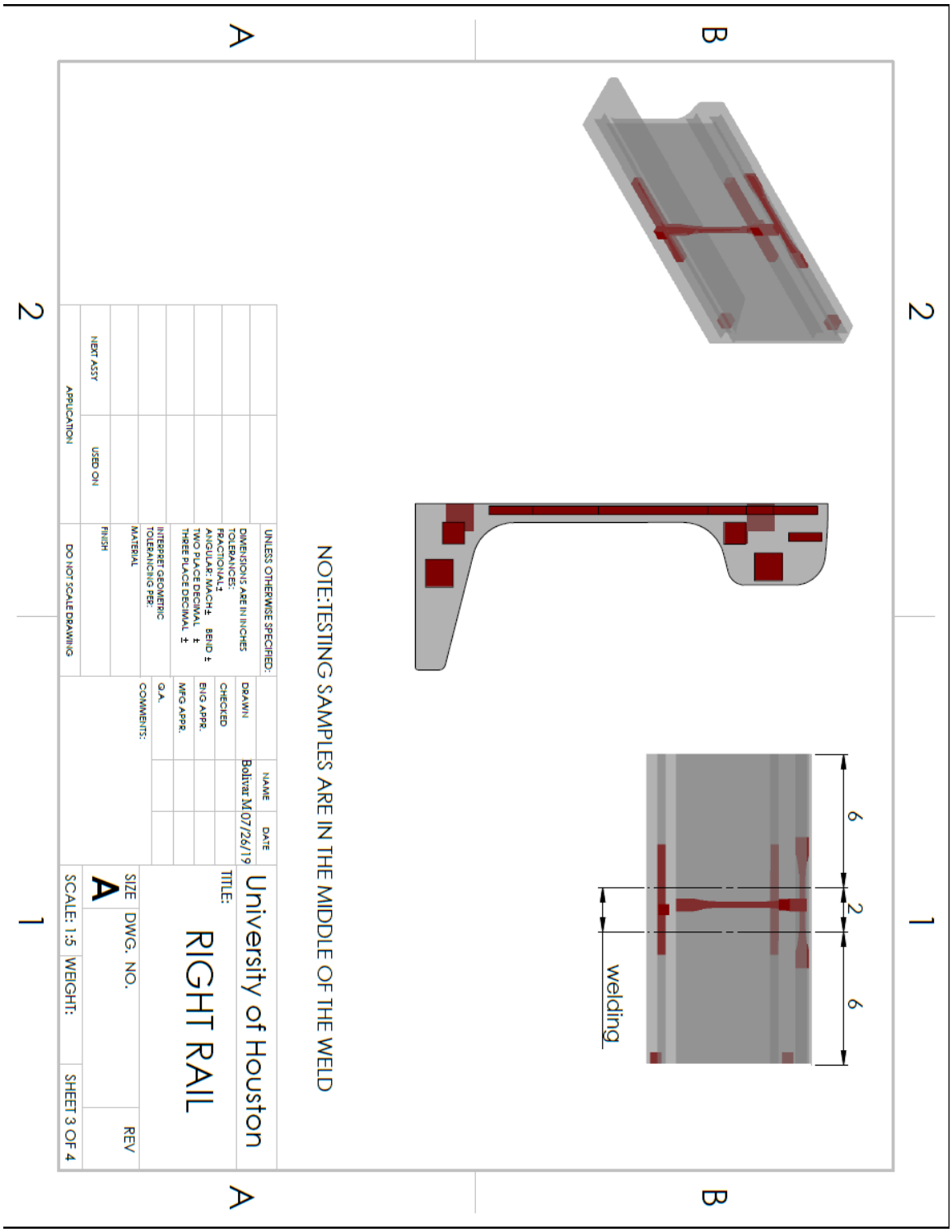

Figure A 12. Different view when compared to Figure 8 for mechanical testing and sample extraction.